Applied Catalysis B: Environmental 125 (2012) 206–214

Contents lists available at SciVerse ScienceDirect

Applied Catalysis B: Environmental

journal homepage: www.elsevier.com/locate/apcatb

Effect of molybdenum addition on supported platinum catalysts for the water–gas shift reaction

W. Damion Williams[a], Luis Bollmann[a,1], Jeffrey T. Miller[b], W. Nicholas Delgass[a], Fabio H. Ribeiro[a,*]

[a] School of Chemical Engineering, Purdue University, West Lafayette, IN 47907, USA
[b] Chemical Technology Division, Argonne National Laboratory, 9700 S. Cass Avenue, Argonne, IL 60439, USA

ARTICLE INFO

Article history:
Received 27 February 2012
Received in revised form 18 May 2012
Accepted 25 May 2012
Available online 4 June 2012

Keywords:
Water–gas shift
X-ray absorption Spectroscopy
Platinum
Molybdenum oxide
PtMo Alloy

ABSTRACT

The effect of molybdenum on water–gas shift ($CO + H_2O \leftrightarrow CO_2 + H_2$) turnover frequencies was investigated for 2 wt% platinum, up to 11 wt% molybdenum, alumina and silica supported catalysts. The maximum PtMo turnover frequencies were observed for Mo weight loadings of 1.4% and 1.2% when supported on Al_2O_3 and SiO_2, respectively. Above these loadings, the exposed Pt surface area as measured by hydrogen chemisorption was reduced. The hydrogen chemisorption values and X-ray absorption spectroscopy of the reduced catalysts indicate the formation of PtMo bimetallic particles that are surface rich in Mo, yet increases in Pt–Mo coordination do not correlate with changes in turnover frequency, and most of the Mo is present in the form of Mo-oxide. The decrease in TOF from the optimum Mo loading is attributed to differences in surface coverages of intermediates that are observed in the changing reaction orders and ascribed to the interplay between the PtMo alloy metal function and the promotion of water activation by MoO_x promotion of the support. The decreased Pt dispersion and CO binding energy of Pt–Mo catalysts result in CO reaction orders as high as 0.8 at 300 °C, and Mo addition resulted in apparent activation energies which were 20–40 kJ/mol lower than the Mo free samples. The promoted catalysts achieved higher TOF than Pt/CeO_2 when calculated at or below 250 °C with 6.8% CO, 8.5% CO_2, 21.9% H_2O, 37.4% H_2, and balance Ar at 1 atm total pressure.

1. Introduction

The water–gas shift (WGS) reaction, $CO + H_2O \leftrightarrow CO_2 + H_2$, is critical in the processing of carbonaceous materials into pure hydrogen fuel. It provides the desirable key steps of converting unreacted CO into CO_2 while producing the more useful H_2. The industrial $Cu–ZnO/Al_2O_3$ catalysts typically used for low temperature WGS are pyrophoric and require a controlled reduction process prior to operation, which makes them non-ideal for on-board fuel reforming [1–3]. Consequently, significant research has been invested on alternative catalysts. Specifically, Pt and Au supported catalysts have been of interest because of the relatively large rates per mole of metal which have been reported. However, the rate per mole of metal for Au and Pt when supported alone on SiO_2 and Al_2O_3 supports is significantly lower than when the metal is supported on reducible oxides. To gain the material benefit of using Al_2O_3 or SiO_2 supports but achieve the high rates of Au and Pt supported on reducible oxides, several studies have investigated the use of promoters [4,5]. In this study, we report the results of using Mo as a promoter for Pt supported on Al_2O_3 and SiO_2.

The use of molybdenum as an additive in WGS catalysts has been studied by several groups. Gorte et al. [6,7] studied the addition of Mo to Pd/CeO_2 catalysts, and found that Mo acted as a poison to the catalyst. The rate per gram of catalyst for Pd/CeO_2 was nearly two orders of magnitude higher than the rate for Pd/MoO_3, and the rate of Pd/CeO_2 was observed to decrease with 0.5 wt% addition of Mo. The 0.5 wt% loading was reported to give 0.54 Mo atoms/nm^2 for a CeO_2 catalyst with a BET surface area of 58 m^2/g [7]. In contrast, Mo has been used as a promoter for some Pt catalysts [8,9]. It has been proposed that the formation of a PtMo alloy is essential to the high activity of the Mo promoted catalyst and that exposure to water disrupts the alloy over time [10].

Studies related to electro-catalysis on PtMo alloys of varying compositions have been performed due to the increased resistance to CO poisoning that Mo provides [11–18]. Both experimental and DFT studies have shown that the strength of CO adsorption is decreased for PtMo alloys [14–17]. It has been hypothesized that CO binding strength is an important descriptor for water–gas shift activity [19], so it is possible that the decrease in CO binding energy

* Corresponding author at: School of Chemical Engineering, Purdue University, 480 Stadium Mall Drive, West Lafayette, IN 47907-2100, USA. Tel.: +765 494 7799.
E-mail address: fabio@purdue.edu (F.H. Ribeiro).
[1] Present address: The Dow Chemical Company, Hydrocarbons Research, B-251 Building, Freeport, TX 77541, USA.

0926-3373/$ – see front matter © 2012 Elsevier B.V. All rights reserved.
http://dx.doi.org/10.1016/j.apcatb.2012.05.037

may play a role in the increased reaction rate observed with the Mo promoter. In their work on model catalyst surfaces, Rodriguez and co-workers [20] found that Cu and Au on MoO_2 supports prepared from a Mo (1 1 0) substrate had higher rates per surface area than CeO_2 supported catalysts. Thus, Mo has the potential to play a role in affecting both the metal and the support functions for Pt based WGS catalysts.

Here we report the rates of $PtMo/Al_2O_3$ and $PtMo/SiO_2$ catalysts for the forward WGS reaction measured at 6.8% CO, 8.5% CO_2, 21.9%H_2O, and 37.4% H_2 at 1 atm total pressure. Hydrogen chemisorption is used to report a TOF by normalizing the rates to the amount of surface Pt. We investigated the effect of Mo using catalysts with Mo:Pt atomic ratios varying from 0 to 13. The use of two different supports aids in the data analysis as the Mo–support interactions are expected to be different and cause the oxidation state and dispersion of the Mo to be different on the alumina versus the silica. Also, the TOFs of the molybdenum free Pt/SiO_2 and Pt/Al_2O_3 are different as a result of a support effect [4]. The cause of the support effect in water–gas shift is still debated in literature, but it has been attributed to several causes such as differences in water dissociation, oxygen vacancies, hydroxyl groups, atomic dispersion of the metal, and the stability of surface intermediates on the different supports [2,5]. X-ray absorption spectroscopy (XAS) was used to study the state of the Mo after different pretreatment conditions and to identify the nature of the interaction between Pt and Mo in the supported catalysts.

2. Materials and methods

2.1. Catalyst preparation

The precursors used to prepare the catalysts were $Pt(NH_3)_4(NO_3)_2$ (PtTA) and ammonium heptamolybdate (AHMo). The silica support used was Davisil 644 from Sigma–Aldrich with a BET surface area of 280 m^2/g, a pore volume of 1.15 mL/g, and an average pore diameter of 15 nm. For the 4.3% Pt/SiO_2 catalyst, 50 g of SiO_2 was slurried in 250 mL H_2O. The pH was adjusted to about 10 by addition of 2 mL of concentrated NH_4OH. Separately, 5.0 g of PtTA was dissolved in 200 mL H_2O and 1 mL NH_4OH. The PtTA solution was rapidly added with stirring to the silica at room temperature. After 15 min, the solution was filtered, re-slurried (twice) in 200 mL H_2O and re-filtered. The $PtMo/SiO_2$ catalysts were prepared by dissolving AHMo in 10 mL H_2O plus 1 mL NH_4OH to impregnate 11 g of SiO_2. 0.24, 1.0, and 2.0 g of AHMo were used to prepare the $PtMo/SiO_2$ samples with 1.2, 4.2, and 9.0 wt% Mo respectively. The catalysts were dried at 110 °C and calcined at 300 °C for 3 h. 0.44 g of PtTA in 10 mL H_2O plus 1 mL NH_4OH was added to the Mo/SiO_2 catalysts. The catalysts were then dried at 110 °C and calcined at 225 °C for 3 h.

The alumina support used was a high-purity γ-Al_2O_3, Pural/Catapal from Sasol, which was calcined at 500 °C before metal precursors were added. The γ-Al_2O_3 had a BET surface area of 200 m^2/g, a pore volume of 0.55 mL/g, and an average pore diameter of 9 nm. For the 2.6% Pt/Al_2O_3 catalyst, 4.5 g PtTA in 23 mL H_2O was added to 45 g Al_2O_3. The catalyst was dried and calcined at 450 °C. The 1.8 wt% Pt, 0.63 wt% Mo/Al_2O_3 catalyst was prepared by dissolving 0.12 g AHMo in 6 mL H_2O plus 1 mL NH_4OH to impregnate 11 g of Al_2O_3. The $PtMo/Al_2O_3$ samples with 1.4, 3.4, 7.5, and 10.7 wt% Mo were prepared by dissolving 0.15, 0.4, 1.0, or 1.5 g of AHMo in 3 mL H_2O plus 1 mL NH_4OH to impregnate 6 g of Al_2O_3. A 7.5% Mo/Al_2O_3 sample with no Pt was prepared by dissolving 1.1 g of AHMo in 3 mL H_2O plus 1 mL NH_4OH to impregnate 6 g of Al_2O_3. The Mo/Al_2O_3 mixtures were dried at 110 °C and calcined at 300 °C for 3 h. For the 1.8 wt% Pt, 0.63 wt% Mo/Al_2O_3 sample, 0.44 g of PtTA in 6 mL H_2O plus 1 mL NH_4OH was added to the Mo/Al_2O_3. Mixtures of 0.25 g of PtTA in 6 mL H_2O plus 1 mL NH_4OH were used to prepare the other $PtMo/Al_2O_3$ samples. After Pt addition, the catalysts were dried at 110 °C and calcined at 300 °C for 3 h.

The CeO_2 support used was prepared by heating cerium (III) acetate hydrate (Aldrich) to 425 °C and holding for 24 h in air. To 10.0 g of CeO_2 was added 0.30 g of PtTA in 5 mL H_2O. The catalyst was dried at 110 °C and calcined in flowing air at 225 °C for 3 h. All catalysts were pre-reduced by heating from room temperature to 250 °C in H_2 and cooling in He. The weight loadings of each catalyst were determined by ICP elemental analysis.

2.2. Kinetic experiments

The kinetic testing apparatus is described in the supporting material. For each of the kinetic experiments, 200–1000 mg of catalyst was added to the reactor. The catalyst was sieved to obtain a particle size between 0.12 and 0.25 mm. Before the start of the water–gas shift experiments, the catalysts were heated to between 100 and 150 °C in 50 sccm of argon gas. The catalysts were reduced by flowing 50 sccm of a 25% H_2/Ar mixture and using a temperature ramp of 5 °C/min to increase the temperature to between 275 and 350 °C. After 2 h of reduction, the catalyst was exposed to a standard water–gas shift composition of 6.8% CO, 8.5% CO_2, 21.9% H_2O, and 37.4% H_2, with the balance being Ar. Under the standard gas composition, the catalyst was held at the reduction temperature to achieve a stable rate. The time used to stabilize the different catalysts was varied, though a typical time of 20 h was used. After stabilization, the temperature of the reactor was altered so that the conversion would be around 5% under the standard conditions. The errors in our measurements of the rate per gram of catalyst are ±15% and are based on our long experience with the unit.

For all kinetic experiments, the total pressure was kept constant at ambient pressure with a total inlet flow rate of 75.4 sccm. Reaction orders for the reactant and product gases were determined by varying each gas concentration individually. The four concentrations were varied over the ranges 4–21% CO, 5–25% CO_2, 11–34% H_2O, and 14–55% H_2 while keeping the total gas flow rate to the reactor constant by varying the concentration of Ar gas. To determine the apparent activation energy, the temperature was varied over a range of 30 °C with the catalyst exposed to the standard gas concentrations.

2.3. Platinum surface area

For the $PtMo/Al_2O_3$, $PtMo/SiO_2$, and Pt/CeO_2 samples, the platinum surface area of the used samples (after the WGS reaction) was measured by H_2 chemisorption. The procedure consisted of reduction at 300 °C for 4 h by flowing Pd-membrane-purified H_2 followed by system evacuation at 300 °C. After evacuation, the sample was cooled to 35 °C prior to analysis. The experiments on the $PtMo/Al_2O_3$ and $PtMo/SiO_2$ samples were performed in a standard volumetric Micromeritics ASAP 2020 instrument. The experiments on the Pt/CeO_2 were performed in an in-house devised standard volumetric apparatus. A Pt/H stoichiometry of 1 was used to estimate the Pt surface area from the value for the volume of gas adsorbed when extrapolated to zero pressure.

For the used Pt/Al_2O_3 and Pt/SiO_2 samples, the platinum surface area was measured by CO chemisorption in the standard volumetric Micromeritics ASAP 2020 instrument. The procedure consisted of reduction at 300 °C for 2 h by flowing Pd-membrane-purified H_2 followed by system evacuation at 300 °C. After evacuation, the sample was cooled to 35 °C prior to analysis.

2.4. XAS measurements

X-ray absorption measurements were conducted on the insertion device beamline of the Materials Research Collaborative Access Team (MRCAT, 10-ID) at Advanced Photon Source (APS), Argonne National Laboratory. Ionization chambers were optimized for the maximum current with linear response (ca. 10^{10} photons detected per s) using a mixture of He, N_2 and Ar gases for 10% and 70% absorption in I_o and I_t, respectively. A third detector in the series collected a reference spectrum (Pt or Mo foil) simultaneously with each measurement for energy calibration. Catalyst samples were pressed into a cylindrical holder with a thickness chosen to give a total absorbance (μx) at the Pt-L_3 (11.56 keV) edge or Mo-K (20.00 keV) edge of about 2.0 and an edge step (μx) of ca. 0.5. The EXAFS and XANES spectra of the PtMo catalysts used in the kinetic experiments were first obtained under atmospheric conditions at room temperature (RT). The samples were then re-reduced at 300 °C for 30 min in 4% H_2/He followed by He purge at 300 °C, and cooled to RT in a continuous-flow EXAFS reactor cell. The spectra were then obtained at RT under static He atmosphere.

2.4.1. XAS data analysis

Phase shift and backscattering amplitudes were obtained from the Mo and Pt foils for Mo—Mo and Pt—Pt scattering, respectively. For Pt–Mo and Mo—Pt, the phase and amplitude files were calculated with FEFF. Standard procedures based on WINXAS 3.1 software were used to fit the XAS data. The EXAFS coordination parameters were obtained by a least squared error fit in R-space of the isolated nearest neighbor, k^2-weighted Fourier transform data. The quality of the fits were equally good with both k^1 and k^3 weightings. XANES references were obtained from the Mo foil as well as powder samples of MoO_2, MoO_3, and Na_2MoO_4. The Mo-K edge energy was evaluated from the maximum of the first derivative of the XANES signal.

2.5. O_2 uptake experiments

The oxygen uptake of the used $PtMo/Al_2O_3$ and $PtMo/SiO_2$ samples was determined for the reduced samples using a Micromeritics ASAP 2020 instrument. The procedure was to reduce the catalysts at 300 °C for 4 h, evacuate the system, cool to 35 °C, and analyze the O_2 chemisorption uptake at different pressures. To provide a uniform analysis of all of the samples which is free from linear extrapolation, the O_2 uptake value at 130 mmHg is reported.

Because the analysis described is not typical for oxygen chemisorption experiments, the uptake data for each experiment is shown in the supporting material.

3. Results

3.1. Reaction rates and kinetics

The apparent activation energies and the rates per mole of Pt for the $PtMo/Al_2O_3$ and $PtMo/SiO_2$ samples are shown in Table 1. The rates were extrapolated to 270 °C, using the measured apparent activation energies, in order to objectively compare the catalysts at a single temperature. A graph of the rates per total mole of Pt at 270 °C is shown in Fig. 1. The weight loadings of the samples range from 0.6 to 10.7 wt% Mo. The moles of CO converted per second per gram of catalyst for the 7.5% Mo/Al_2O_3 sample equaled 5×10^{-8} at 377 °C, so the contribution from the rate for oxidized molybdenum is not considered to affect the promotion of the catalyst. However, if oxidized molybdenum covered all of the platinum, the rate per gram of catalyst may be expected to approach numbers similar to the Mo/Al_2O_3 samples.

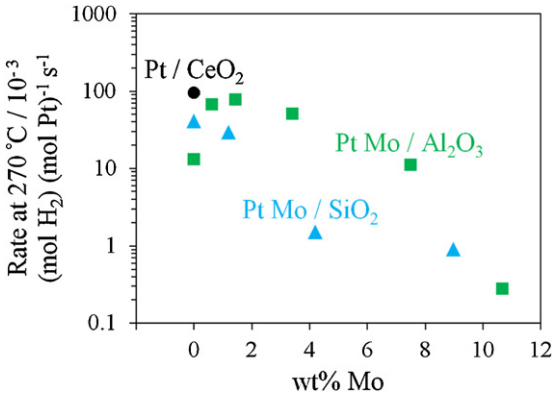

Fig. 1. Rate per total mole of platinum versus wt% of molybdenum for Pt/SiO_2 (triangles), Pt/Al_2O_3 (squares), and Pt/CeO_2 (circle). All rates are calculated at 270 °C, 6.8% CO, 21.9% H_2O, 8.5% CO_2, and 37.4% H_2.

The maximum in the rate per mole of Pt calculated at 270 °C was observed when the weight loading of molybdenum was between 0.6 and 3.4 wt% for the alumina supported catalysts. Also, the maximum rates per mole of Pt observed for the $PtMo/Al_2O_3$ are similar to that from a Pt/CeO_2 catalyst when extrapolated to 270 °C. Upon the addition of Mo at or above 3.4 wt%, the rate per mole of Pt started to decrease. The largest decrease in rate was observed for the 2% Pt, 10.7% Mo/Al_2O_3 sample, which had a nearly two orders of magnitude lower rate per mole of Pt than the Mo free sample. No enhancement in the rate per mole of Pt at 270 °C was observed for the Pt/SiO_2 series and the rate decreased by 25% with as little as 1.2 wt% Mo.

The dispersion of the platinum, as measured by hydrogen chemisorption, was affected by the addition of Mo (Table 1). For alumina supported catalysts, the Pt dispersion of the 7.5 wt% Mo sample was nearly half of that for the 1.4 wt% Mo sample, 31% versus 18%. On the other hand, a sharper decline in the Pt dispersion occurred when changing the loading of Mo from 1.2 wt% to 4.2 wt% and 9 wt% in the silica supported catalysts, 11% versus 1.5% and 3.2% respectively. It is the low dispersion of the $PtMo/SiO_2$ samples that is responsible for the low rate per total mole of Pt. As observed from Tables 1 and 2, the rate per total mole of Pt and the rate per gram of catalyst decreased as the Pt became less accessible to the reactant gases. Still, the dispersion of the Pt metal on the different supports was considerably different even with similar weight loadings of molybdenum. Thus, by normalizing the rate to the amount of available surface Pt as measured by chemisorption, a better comparison of the rates to one another was achieved [21]. The turnover frequency (TOF) for this system is reported as the moles of H_2 produced per surface mole of Pt per second.

In Fig. 2, the TOF of the different catalysts calculated at 270 °C is plotted as a function of the weight loading of Mo. Although the rate per total mole of Pt for the silica supported catalysts was not enhanced with Mo addition, the TOF at 270 °C was enhanced with up to 4 wt% Mo. For both the alumina and silica supported catalysts, the TOF shows a maximum below 4 wt% Mo. The trends in the rate per total mole of Pt for the alumina and silica supported catalysts are very different, yet the TOFs follow a similar trend. The maximum TOF values observed are very similar to one another, and are greater than 10 times the TOF observed on the Pt/Al_2O_3 catalyst. Consequently, the calculated TOFs at 270 °C for the best $PtMo/Al_2O_3$ and $PtMo/SiO_2$ catalysts are comparable to that observed for Pt/CeO_2.

The apparent activation energies of the PtMo catalysts ranged from 42 to 63 kJ/mol, which were all lower than those observed on the Mo free Pt catalysts, 74 to 82 kJ/mol. The reaction orders had the largest changes when the rate per gram of the catalyst was significantly decreased and the catalysts had to be tested at higher

Table 1
Molybdenum affects the dispersion and kinetics of the WGS reaction for Pt/SiO_2 and Pt/Al_2O_3 catalysts.

Support	Pt/wt%	Pt dispersion	Ea/kJ mol^{-1}	Rate[e]/$\times10^{-3}$ (mol H_2) (mol Pt)$^{-1}$ s^{-1}	TOF[e]/$\times10^{-3}$ (mol H_2) (surface mol Pt)$^{-1}$ s^{-1}
SiO_2	4.3	48[c]	74	40	85
1.2% Mo/SiO_2	1.9	11[d]	48	29	260
4.2% Mo/SiO_2	1.8	1.5[d]	50	1.5	100
9.0% Mo/SiO_2	1.8	3.2[d]	42	0.9	28
Al_2O_3	2.6	77[c]	82	13	17
0.63% Mo/Al_2O_3	1.8	38[d]	44	67	150
1.4% Mo/Al_2O_3	2.1	31[d]	47	77	220
3.4% Mo/Al_2O_3	2.2	27[d]	48	51	150
7.5% Mo/Al_2O_3	1.7	18[d]	58	11	54
10.7% Mo/Al_2O_3	1.7	5.9[d]	63	0.3	5
7.5% Mo/Al_2O_3	0	N/A	117	N/A	N/A
CeO_2	1.0	34[d]	78	94	280
2.2% Na/Al_2O_3 [a]	0.65	22[d]	76	350	1600
Mo_2C [b]	3.9	N/A	53	2800	N/A

[a] Data from reference [34].
[b] Data from reference [35]. Rate calculated at 270 °C, 11% CO, 21% H_2O, 6% CO_2, and 43% H_2.
[c] Dispersion of Pt in % was measured by CO chemisorption
[d] Dispersion of Pt in % was measured by hydrogen chemisorption
[e] All rates and turnover frequencies are calculated at 270 °C, 6.8% CO, 21.9% H_2O, 8.5% CO_2, and 37.4% H_2 except for the Pt/Mo_2C sample.

Table 2
The effect of molybdenum on the WGS reaction orders for Pt catalysts.

Support	Pt/wt%	Temp. of orders[b]/°C	Reaction orders				Rate[c]/$\times10^{-8}$ (mol H_2)(g cat)$^{-1}$ s^{-1}
			CO	H_2O	CO_2	H_2	
SiO_2	4.3	189	0.1	0.6	0.0	−0.1	1050
1.2% Mo/SiO_2	1.9	236	0.1	0.8	−0.1	−0.2	314
4.2% Mo/SiO_2	1.8	281	0.5	0.8	−0.1	−0.3	15.2
9.0% Mo/SiO_2	1.8	312	0.8	0.3	−0.4	−0.1	8.8
Al_2O_3	2.6	244	0.1	0.6	0.0	−0.4	205
Al_2O_3 [a]	1.7	300	0.1	0.8	−0.1	−0.5	67
0.63% Mo/Al_2O_3	1.8	165	0.0	0.8	0.0	−0.2	660
1.4% Mo/Al_2O_3	2.1	170	0.0	0.8	−0.1	−0.2	924
3.4% Mo/Al_2O_3	2.2	195	0.1	0.8	−0.1	−0.2	643
7.5% Mo/Al_2O_3	1.7	280	0.3	0.5	−0.1	−0.3	111
10.7% Mo/Al_2O_3	1.7	370	0.8	0.5	−0.7	−0.5	2.7
7.5% Mo/Al_2O_3	0	377	0.8	−0.2	−0.1	0.0	0.09
CeO_2	1.0	215	−0.1	0.9	−0.1	−0.5	587

[a] Data from reference [22].
[b] The reaction orders were measured at the temperature reported.
[c] Rate per gram of catalyst calculated at 270 °C, 6.8% CO, 21.9% H_2O, 8.5% CO_2, and 37.4% H_2.

temperatures, Table 2. After the Mo loading exceeded 4 wt%, it was necessary to test the catalysts at higher temperatures in order to determine the rate accurately. For the low rate catalysts tested at 280 °C and above, there was a clear trend that the carbon monoxide reaction order increased, the water order decreased, and the carbon dioxide order became more negative. Note that the temperatures at which the reaction orders were collected are different for each catalyst, but the kinetics shown here for the PtMo catalysts are distinctly different from those reported in the literature for typical Pt catalysts. Using similar reaction conditions to those reported here, Phatak et al. [22] measured the reaction orders for Pt/Al_2O_3 in the temperature range of 285–315 °C and found CO reaction orders that varied from 0.06 to 0.11 and are similar to the values we report for Pt/Al_2O_3 and Pt/SiO_2. In contrast, the PtMo catalysts had CO reaction orders as high as 0.8 in the same temperature range.

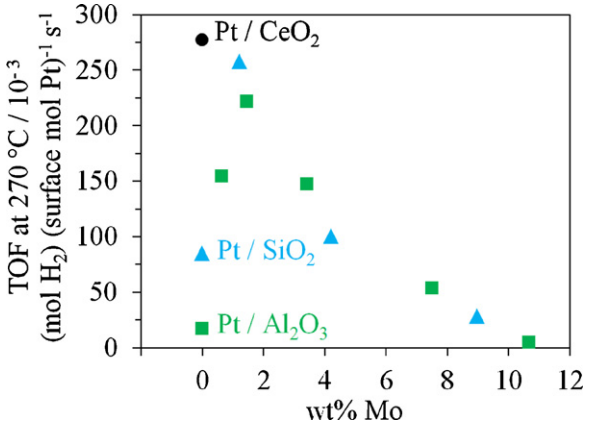

Fig. 2. TOF as determined by hydrogen or CO chemisorption versus wt% of molybdenum for Pt/SiO_2 (triangles), Pt/Al_2O_3 (squares), and Pt/CeO_2 (circle). All rates are calculated at 270 °C, 6.8% CO, 21.9% H_2O, 8.5% CO_2, and 37.4% H_2.

3.2. X-ray absorption spectroscopy

The results of the XAFS fittings for the used catalysts after in situ reduction and after exposure to air are shown in Table 3. The Pt, 1.2% Mo/SiO_2 sample showed both Pt—Pt and Pt—O coordination after exposure to air. The Pt—Pt coordination after reduction for the same sample was also the largest of any of the samples. Both of these results indicate a larger Pt particle size compared to the other samples. Negligible Pt–Mo coordination was observed after the samples were exposed to air and all of the samples except the Pt, 1.2% Mo/SiO_2 sample showed predominantly Pt—O bonds. For the Al_2O_3 supported catalysts, the Pt—O coordination was approximately the same or decreased as the weight loading of Mo was

Table 3
Summary of coordination number (N), bond distance (R), Debye–Waller factor ($\Delta\sigma^2$), and energy correction factor (Eo) obtained from fitting results of the Pt-L_3 edge EXAFS experiments for the 2 wt% Pt, X wt% Mo/SiO_2 or Al_2O_3 samples.

Sample	Treatment	Scatter	N	R/Å	$\Delta\sigma^2/\times10^{-3}$	Eo/eV
Pt, 1.2% Mo/SiO_2	H_2 300 °C	Pt–Pt	8.0	2.77	1	−2.0
		Pt–Mo	1.9	2.75	1	12.5
	Air RT	Pt–Pt	3.6	2.73	1	−2.4
		Pt–O	2.5	2.05	2	1.7
Pt, 4.2% Mo/SiO_2	H_2 300 °C	Pt–Pt	5.7	2.77	1	−2.4
		Pt–Mo	3.0	2.75	1	10.6
	Air RT	Pt–O	3.2	2.05	2	2.1
Pt, 9.0% Mo/SiO_2	H_2 300 °C	Pt–Pt	6.0	2.77	1	−3.0
		Pt–Mo	3.0	2.75	1	11.6
	Air RT	Pt–O	3.1	2.05	2	2.8
Pt, 0.63% Mo/Al_2O_3	H_2 300 °C	Pt–Pt	5.3	2.73	2	−1.7
		Pt–Mo	1.0	2.71	2	9.1
	Air RT	Pt–O	3.7	2.05	2	1.0
Pt, 1.4% Mo/Al_2O_3	H_2 300 °C	Pt–Pt	5.9	2.73	2	−2.8
		Pt–Mo	1.2	2.71	2	12.1
	Air RT	Pt–O	3.3	2.05	2	1.6
Pt, 3.4% Mo/Al_2O_3	H_2 300 °C	Pt–Pt	5.8	2.73	2	−2.8
		Pt–Mo	1.6	2.71	2	11.1
	Air RT	Pt–O	3.2	2.06	2	2.1
Pt, 7.5% Mo/Al_2O_3	H_2 300 °C	Pt–Pt	5.4	2.73	2	−2.7
		Pt–Mo	2.5	2.71	2	10.8
	Air RT	Pt–O	3.4	2.04	2	0.8
Pt, 10.7% Mo/Al_2O_3	H_2 300 °C	Pt–Pt	6.2	2.73	2	−3.5
		Pt–Mo	2.7	2.71	2	10.9
	Air RT	Pt–O	2.5	2.05	2	1.5

increased. This, along with the approximately constant Pt–Pt coordination number, indicates that the actual Pt particle size does not change considerably on the different Al_2O_3 catalysts.

For both the Al_2O_3 and SiO_2 supported catalysts, the average Pt–Mo coordination was lowest for the samples with the lowest weight loading of Mo. The Pt–Mo coordination for the Pt, 1.2% Mo/SiO_2 and the Pt, 1.4% Mo/Al_2O_3 samples were 1.9 and 1.2 respectively. In general, for similar weight loadings of Mo, the Pt–Mo coordination was slightly higher for the SiO_2 supported samples. The Pt–Mo effective bond distances of 2.71–2.75 Å were very similar to the Pt–Pt distances of 2.73–2.77 Å. The lowest ratio observed for Pt–Pt and Pt–Mo coordination was 2 to 1. For the Al_2O_3 supported samples after reduction, the Pt-Mo coordination number was observed to increase with Mo loading. The increase in Pt–Mo coordination occurred along with the decrease in dispersion as measured by hydrogen chemisorption, and the results suggest that the Pt–Mo coordination could be due to the formation of a PtMo bimetallic particle that is surface rich in molybdenum. Furthermore, the low Pt–Mo coordination numbers in the reduced catalysts and the absence of Pt–Mo scatters in the air oxidized samples suggest that most of the Mo is at the nanoparticle surface.

Results of the XAFS fittings for the Mo-K edge of the reduced samples further support the idea of PtMo bimetallic particles with the surface enriched by Mo. For the Pt, 1.2% Mo/SiO_2 sample, a peak for Mo–Mo scattering was present with an effective distance of 2.74 Å. However, this peak becomes difficult to detect with increases in Mo loading because most of the Mo was present as a form of Mo-oxide (Table S1). The total Mo metallic coordination number (Mo–Mo and Mo–Pt) was much smaller than the total Pt coordination number which is consistent with a surface enriched by Mo. An example of the Fourier transform of the XAFS data showing the different Mo peaks is shown in Fig. S1. Mo–Pt coordination was present in each $PtMo/SiO_2$ sample, but its contribution to the overall signal was observed to decrease with increases in Mo loading as a higher percentage of the Mo was present in the form of the oxide. Any Mo–Pt peaks for the Al_2O_3 supported samples were too small to fit, because most of the Mo was present in the form of an oxide and did not have significant contact with the Pt as compared to the SiO_2 supported samples.

The nature of the Mo-oxide was analyzed by examining the XANES of the Mo-K edge spectra for the $PtMo/Al_2O_3$ and $PtMo/SiO_2$ samples in air and after reduction. Examples of the spectra for two of the catalysts are shown in Fig. 3. An analysis of the average state of oxidation for the molybdenum was performed by examining the first derivative of the XANES, Fig. 4, and comparing the edge positions to the positions for known spectra, Table S2. When the PtMo samples were exposed to air at room temperature, the Mo edge energy was near 20 016.5 eV which is in between the edge energies of 20 016 eV for MoO_3 and 20 017.5 eV for Na_2MoO_4. Thus, all of the samples exposed to air had mostly Mo (VI).

After the $PtMo/SiO_2$ samples were reduced, there were significant changes to the edge energies similar to those shown in Fig. 3. The edge energy of Mo in the reduced $PtMo/SiO_2$ samples was near 20 014.5 eV. Based on the additional information from the XAFS, we attribute the shift in edge energy to reduction of Mo (VI) to a mixture of Mo-oxides and Mo^0. The edge energy of MoO_2 is 20 014 eV, so the reduction of the Mo (VI) to a large amount of MoO_2 could explain the changes in the XANES for the $PtMo/SiO_2$ samples. Conversely, the $PtMo/Al_2O_3$ samples show significantly smaller changes in the XANES and the edge energy remains near 20 016 eV as shown in Fig. 3. While there is reduction of the Mo in the $PtMo/Al_2O_3$ samples, much of the Mo remains as Mo (VI).

3.3. O_2 uptake experiments

Oxygen chemisorption experiments were performed on the used PtMo catalysts after their in situ reduction as described in Section 2.5. The oxygen uptake was not solely due to chemisorption of oxygen on Pt because the uptake values at high Mo loadings were larger than what is possible for oxidation of the Pt. As observed from the XAS results, some of the Mo was reduced at 300 °C and the high oxygen uptake values indicate that reduced Mo was oxidized

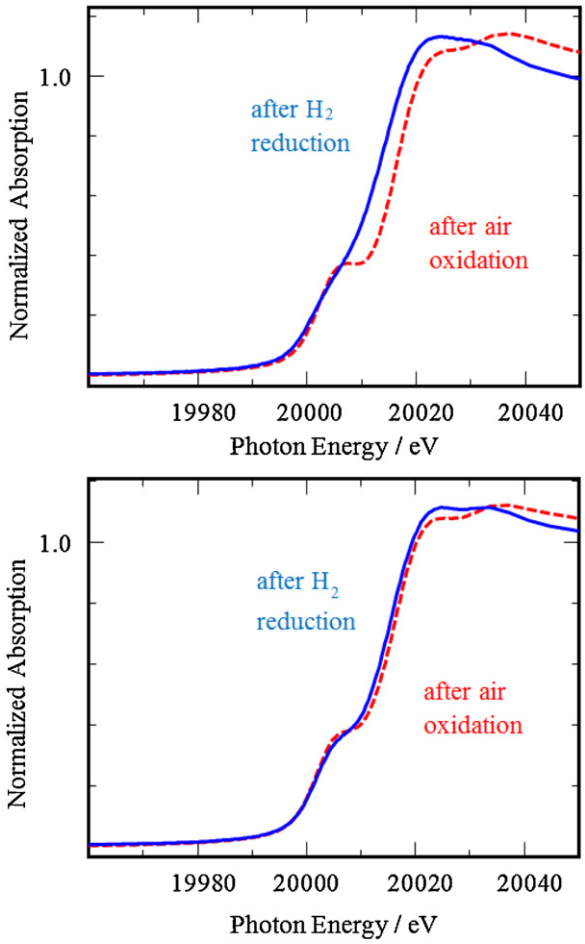

Fig. 3. Mo K-edge XANES from 19 960 to 20 050 eV for Pt, 4.2% Mo/SiO_2 (top) and Pt, 1.4% Mo/Al_2O_3 (bottom). Spectra for samples after reduction (solid blue lines) were collected in helium at room temperature after the samples were reduced at 300 °C in flowing H_2 for 30 min. The spectra for samples after air oxidation (dotted red lines) were collected in air at room temperature. (For interpretation of the references to color in this figure legend, the reader is referred to the web version of the article.)

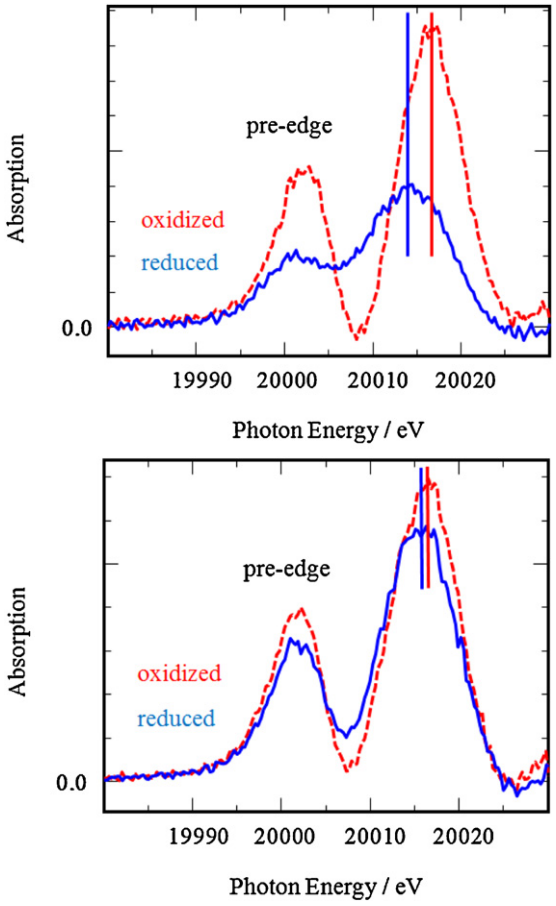

Fig. 4. First derivative of the Mo K-edge XANES from 19 980 to 20 030 eV for 2% Pt 4.2% Mo/SiO_2 (top) and 2% Pt 1.4% Mo/Al_2O_3 (bottom). Dotted red line: sample in air. Solid blue line: sample after reduction at 300 °C. (For interpretation of the references to color in this figure legend, the reader is referred to the web version of the article.)

during the experiments. If 2 wt% Pt was oxidized to PtO, the uptake amount of O_2 at STP would be 1.15 cm^3/g of catalyst. If 10 wt% Mo was oxidized from MoO_2 to MoO_3, the uptake amount would be 11.7 cm^3/g of catalyst. The Al_2O_3 and SiO_2 samples which showed the largest oxygen uptakes had values of 2.1 and 6.6 cm^3/g of catalyst respectively. The results in Fig. 5 show that the reducible sites on the $PtMo/Al_2O_3$ samples increased with Mo loading up to a maximum for the sample with 7.5 wt% Mo. In contrast, the $PtMo/SiO_2$ samples show rather linear behavior in the amount of reducible Mo even up to 9 wt% Mo, and the amount of reducible Mo for the 9 wt% Mo sample was over 3 times that observed for the $PtMo/Al_2O_3$ samples.

4. Discussion

The promotion of the Pt/Al_2O_3 and Pt/SiO_2 catalysts by Mo was accompanied by a change in kinetics on each support. As shown in Table 1, there is a clear trend that the apparent activation energy is lower by 20 to 40 kJ/mol compared to that for Pt only catalysts for all of the samples which are promoted by Mo. Consequently, the difference in the relative rates between the Mo-containing samples and Mo-free samples will increase as the temperature is decreased, and the Mo-containing samples will have higher relative rates. A comparison of the TOF for the best PtMo catalysts to the Mo-free Pt catalysts is shown in Fig. 6.

As the amount of Mo increased to 3.4 wt% on Al_2O_3 and 4.2 wt% on SiO_2 a decrease in the TOF was observed, as shown in Table 1. Because the TOF decreases, it is clear that the role of Mo in generating sites is complex, and that it is necessary to refine the explanation for how Mo affects the structure of the catalyst and promotes the Pt.

As the Mo loading increased, the Pt–Mo coordination increased and the oxygen uptake of the reduced catalysts tended to be higher. The reducibility of the molybdenum oxide on each support is expected to depend on its structure. A loading of 15 wt% Mo corresponds to monolayer coverage for an Al_2O_3 support with a surface area of 200 m^2/g (assuming monolayer surface coverage of 4.6 Mo/nm^2) [23]. Small loadings of Mo, ca. 0.2 Mo atoms/nm^2, are expected to produce isolated monomolybdate species after dehydration. On the other hand, higher loadings near monolayer coverage can produce monomolybdate as well as polymolybdate structures [23]. Isolated monomolybdate has been observed after dehydration below 0.8 Mo/nm^2 on SiO_2. However, the Mo is not expected to interact as strongly with the SiO_2 and is expected to form MoO_3 crystallites at loadings above 0.8 Mo/nm^2. This means that the formation of crystallites will occur above a weight loading of 3.6 wt% for a SiO_2 support with a surface area of 280 m^2/g [23].

Molybdenum oxide typically begins reduction at lower temperatures and reduces to a lower oxidation state as the loading of molybdenum increases on the Al_2O_3 support and MoO_3 crystallites are formed [24,25]. The exception is that at high loadings of Mo above monolayer coverage, TPR experiments indicate polymolybdate reduction starts at a lower temperature than MoO_3

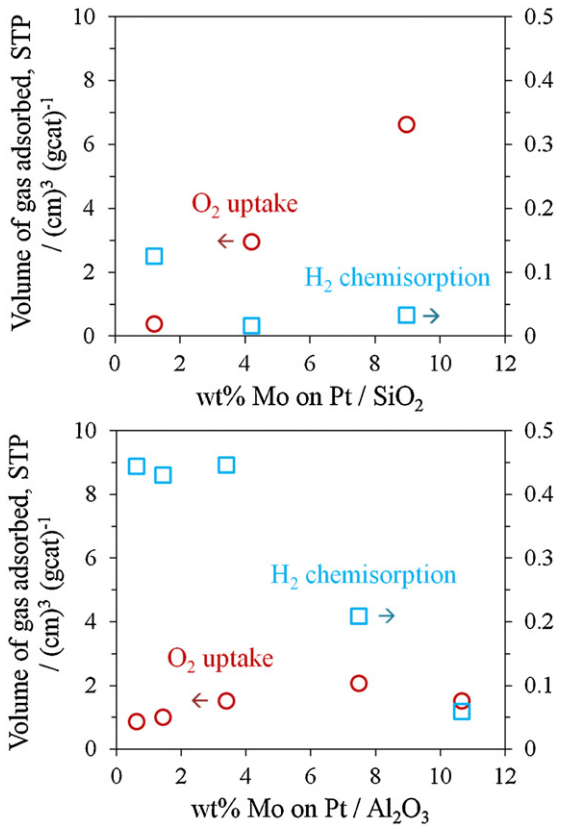

Fig. 5. Results of oxygen uptake experiments for $P(O_2)$ = 130 mmHg at 35 °C following hydrogen reduction and evacuation at 300 °C (circles). Hydrogen chemisorption at 35 °C was performed on the catalysts after reduction and evacuation at 300 °C. The volume of chemisorbed gas is the value extrapolated to zero pressure (squares).

crystallites [26]. Negligible reduction is observed below 573 K at any Mo loading on Al_2O_3 [25,26]. In contrast to Mo-oxide/Al_2O_3, the onset temperature for reduction of Mo-oxide/SiO_2 remains approximately the same regardless of the Mo loading [26,27]. Consequently, Mo-oxide on SiO_2 should reduce more easily than on Al_2O_3 when the surface coverage of Mo is low [25,27]. For Mo-oxide/SiO_2, negligible reduction is observed below 673 K at any Mo loadings [26,27].

The results of the XAS and oxygen uptake experiments follow the trends observed in the literature for MoO_3 supported on Al_2O_3 and SiO_2. After reduction, the Mo displayed a lower oxidation state on SiO_2 than Al_2O_3 due to the weaker Mo–support interaction.

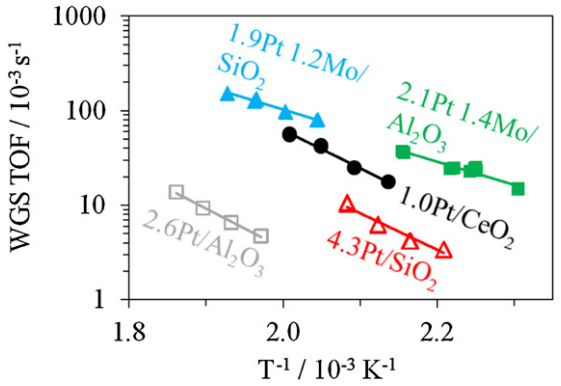

Fig. 6. TOF as determined by hydrogen or CO chemisorption for different water–gas shift catalysts tested under conditions of 6.8% CO, 21.9% H_2O, 8.5% CO_2, 37.4% H_2, and balance Ar.

Furthermore, a higher Pt–Mo coordination was possible on the PtMo/SiO_2 catalysts because the weaker Mo–support interaction means there was more Mo available to add to the PtMo bimetallic particles. The main difference in the results was that the PtMo catalysts were observed to reduce at temperatures well below the onset reduction temperatures typically observed for molybdenum oxide without platinum. Therefore, the Pt is proposed to aid in the reducibility of the Mo species on each catalyst.

The XAFS and XANES of the PtMo catalysts reduced at 300 °C indicate a large portion of the Mo is in an oxidized state with some Mo^0 coordinated to Pt. Based on the chemisorption and XAS results, we have proposed that the Mo^0 forms a PtMo bimetallic particle that is surface rich in Mo. This proposed structure is consistent with the idea that the surface free energy of Pt^0 is expected to be lower than that for Mo^0 but not lower than that for Mo-oxides. Theory regarding near surface alloys has shown that Mo^0 would be expected to distribute into the bulk of the Pt particles [17]. Because oxides typically have lower surface free energies, it is expected that any Mo-oxide would remain on the surface [28]. An alternative explanation for the increase in Pt–Mo coordination with Mo loading is that the Pt particles are resting atop Mo atoms on the support. However, this explanation does not help to explain the decrease in platinum surface area with Mo addition. The expected distance, as determined by density functional theory, for the Pt–Mo bond when Mo is on the surface of a Pt nanoparticle is shorter, at 2.59 Å, than that for the Pt–Mo bond distances (2.71–2.75 Å) reported in [29]. However, with Mo distributed in the bulk of the nanoparticle, an average of the Pt–Mo distances would result in larger average Pt–Mo bond lengths [29]. Pt and Mo have very similar metallic radii, so the Pt–Pt and Pt–Mo bond distances are expected to be similar in some of the bimetallic particles. For example, the $Pt_{0.8}Mo_{0.2}$ alloy has a face-centered cubic (FCC) lattice with a = 3.91 Å while Pt has a FCC lattice with a = 3.92 Å [12] and a nearest neighbor Pt–Pt bulk distance of 2.77 Å.

The Pt–Pt and Pt–Mo coordination numbers have a ratio that varies from a high of 4 to a low of 2. The XAS ratio of Pt–Pt:Pt–Mo coordination numbers for the $Pt_{0.8}Mo_{0.2}$ alloy are approximately 5.1:0.8 [12]. Thus we can conclude that more Mo is incorporated into the bimetallic particles than in the $Pt_{0.8}Mo_{0.2}$ alloys at higher loadings. The bond distances and Pt–Mo coordination numbers are consistent with the incorporation of Mo into the Pt particles to form a Pt_2Mo alloy. However, it is difficult to rule out other stoichiometric alloys such as $Pt_{0.75}Mo_{0.25}$ or PtMo [30,31]. The difficulty in identifying the exact structure arises because the Mo is not distributed in a homogeneous alloy phase due to surface enrichment. In spite of the uncertainty in composition, we conclude that some of the Mo was fully reduced to Mo^0 and formed PtMo bimetallic particles which are surface rich in Mo. Additionally, some of the Mo in close proximity to the Pt is reduced to Mo (IV), some of the Mo is not reduced at all and remains as Mo (VI), and the amount of reduced Mo is higher on SiO_2 than Al_2O_3.

Although the Pt–Mo coordination increased with Mo loading, the TOF was observed to decrease above 3.4 wt% on Al_2O_3 and 4.2 wt% on SiO_2. Consequently, the formation of PtMo bimetallic particles does not show a direct correlation with the TOF. Furthermore, we hypothesize that the active site must have been altered in some way to account for the decrease observed in TOF. The oxidized Mo^{6+} is likely not catalytic as evidenced by the low rate of the Mo/Al_2O_3 catalyst and the decrease in hydrogen chemisorption with increasing Mo addition. Because the Mo^{6+} is not expected to be active, it is hypothesized that the maximum rate of the catalyst should not occur before the Mo is sufficiently reduced. It is reasonable to suspect for this bimetallic system that something about the state of one or both of those metals may have changed. The average state of the Mo is clearly very different on Al_2O_3 as compared to SiO_2 so the TOF trends suggest that only the Mo which interacts

closely with the Pt is important. Upon further inspection, the catalysts which show the highest TOF (0.6Mo, 1.4Mo, 3.4Mo/Al_2O_3 and 1.2Mo/SiO_2) have Pt–Pt to Pt–Mo ratios which vary between 4 and 5. The catalysts with lower TOF (7.5Mo, 10.7Mo/Al_2O_3 and 4.2Mo, 9.0Mo/SiO_2) have ratios of approximately 2.

As the Pt–Mo coordination increased, the dispersion of Pt decreased and the catalyst was tested at higher temperatures due to the lower rate per gram of catalyst. Platinum is typically observed to have a low CO order, near 0, due to the high coverage of CO present under reaction conditions [22,32,33]. The PtMo alloy is expected to decrease the CO bonding strength relative to Pt which would cause the relative coverage of CO to decrease at higher temperatures [14–17]. The changes to the CO order can be explained by the formation of the PtMo bimetallic particles. The lower coverage of CO resulted in the higher reaction order which was observed for the catalysts tested above 280 °C as shown in Table 2. The similarities in the apparent activation energies of the PtMo samples indicate that the active sites and mechanism may be similar for each catalyst. However, it can be concluded that the relative surface coverages on the active sites have changed by virtue of the changes to the reaction orders. Thus, the decrease in TOF can be partially attributed to the differences in surface species on different catalysts, and changes to the partial pressures of gases in the experiment would cause the relative TOFs to change. The changes to the reaction orders are likely to come from the changes in the amount of Mo in the PtMo bimetallic particles or possibly from testing the catalysts at higher temperatures or both.

Although we have discussed details of the structure of the catalyst, it is still necessary to determine whether or not the increase in TOF is caused by the presence of PtMo bimetallic particle sites or by another type of site. The use of in situ XAS, Raman, UV–vis spectroscopy or isotope switching and other transient techniques that might better define the active nature of the Mo could be potentially interesting tools for identifying the mechanism or ways to improve the catalyst performance. The evidence in literature for MoO_2 being a good support material for WGS provides an alternative explanation for the increase in rate observed with Mo promotion from those explanations related to the PtMo alloy or alteration of the metal site. Rodriguez et al. [20] studied Au nanoparticles supported on model MoO_2 surfaces. They proposed that the role of MoO_2 is to enhance the rate through the enhancement of water dissociation. This was considered likely because water dissociation is more difficult on Au nanoparticles where DFT results showed that the activation barrier was approximately 1.3 eV. If the Mo does act to promote the support effect, our results would explain why Gorte et al. found that Mo acts as a poison to Pd/CeO_2 catalysts [7]. CeO_2 is well known as a good support for water–gas shift catalysts. Here we show that Mo promotes the rate of Pt on Al_2O_3 and SiO_2 to be as good as Pt/CeO_2. For this reason, if Mo acts as a support-type promoter, it would not be expected to substantially increase the rate for CeO_2 supported catalysts because the CeO_2 has already enhanced the rate of the metal through the support effect.

MoO_2 or reduced Mo in close proximity to Pt could contribute to the rate by increasing the ability of the support to dissociate water [20]. Further evidence for the Mo providing a support-type effect comes from the PtMo/Al_2O_3 and PtMo/SiO_2 catalysts having similar trends in TOF while the Pt/SiO_2 and Pt/Al_2O_3 catalysts have different rates. In other words, the enhancement of the rate is not cumulative when PtMo is placed on SiO_2. Although the wide temperature over which the kinetic data were collected prevents a full quantitative analysis, the current results suggest that the formation of PtMo bimetallic particles influences the kinetics but that the increase in TOF observed with Mo addition is due to a support-type effect. Finally, the addition of Mo resulted in decreased Pt surface area and an increased CO reaction order which is related to the coverage of CO on the bimetallic particles. The changes to the Pt surface and the corresponding coverages of intermediates provide a possible explanation for the decrease in TOF at higher Mo loadings.

5. Conclusions

Molybdenum-promoted platinum catalysts supported on alumina and silica are reported to have water–gas shift turnover frequencies similar to that of Pt/CeO_2 at gas concentrations of 6.8% CO, 8.5% CO_2, 21.9%H_2O, 37.4% H_2, and balance Ar at 1 atm total pressure and below 250 °C. Characterization of the catalysts using XAS and hydrogen chemisorption identifies the formation of PtMo bimetallic particles that are surface rich in Mo. However, the Pt–Mo coordination of the reduced catalysts did not correlate with the TOF which is observed to decrease by over an order of magnitude at higher Mo loadings. We hypothesize that the increased CO reaction orders on the Pt–Mo catalysts, which were observed at temperatures near 300 °C, are the result of the decrease in CO binding energy for PtMo alloys. The decrease in the TOF is attributed to the resulting changes to the surface coverages caused by the alloy. The similarity of the PtMo/Al_2O_3 and PtMo/SiO_2 TOF advances the hypothesis that reducible Mo-oxide in close proximity to the Pt enhances the rate in a manner similar to the support-type effect observed in the literature for MoO_2 supported catalysts.

Acknowledgments

Support for this research was provided by the U.S. Department of Energy, Office of Basic Energy Sciences, through the Catalysis Science Grant No. DE-FG02-03ER15466. Use of the Advanced Photon Source was supported by the U.S. Department of Energy, Office of Basic Energy Sciences, under contract No. DE-AC02-06CH11357. MRCAT operations are supported by the Department of Energy and the MRCAT member institutions. Partial funding for JTM was supported as part of the Institute for Atom-efficient Chemical Transformations (IACT), an Energy Frontier Research Center funded by the U.S. Department of Energy, Office of Science, Office of Basic Energy Sciences.

Appendix A. Supplementary data

Supplementary data associated with this article can be found, in the online version, at http://dx.doi.org/10.1016/j.apcatb.2012.05.037.

References

[1] R. Farrauto, S. Hwang, L. Shore, W. Ruettinger, J. Lampert, T. Giroux, Y. Liu, O. Ilinich, Annual Review of Materials Research 33 (2003) 1–27.
[2] C. Ratnasamy, J.P. Wagner, Catalysis Reviews: Science and Engineering 51 (2009) 325–440.
[3] R. Burch, Physical Chemistry Chemical Physics 8 (2006) 5483–5500.
[4] P. Panagiotopoulou, D.I. Kondarides, Catalysis Today 127 (2007) 319–329.
[5] Y.P. Zhai, D. Pierre, R. Si, W.L. Deng, P. Ferrin, A.U. Nilekar, G.W. Peng, J.A. Herron, D.C. Bell, H. Saltsburg, M. Mavrikakis, M. Flytzani-Stephanopoulos, Science 329 (2010) 1633–1636.
[6] X. Wang, R.J. Gorte, Applied Catalysis A 247 (2003) 157–162.
[7] S. Zhao, T. Luo, R.J. Gorte, Journal of Catalysis 221 (2004) 413–420.
[8] W. Ruettinger, X.S. Liu, X.M. Xu, R.J. Farrauto, Topics in Catalysis 51 (2008) 60–67.
[9] S.M. Opalka, T.H. Vanderspurt, R. Radhakrishnan, Y. She, R.R. Willigan, Journal of Physics: Condensed Matter 20 (2008) 064237.
[10] L. Dorazio, W. Ruettinger, M. Castaldi, R. Farrauto, Topics in Catalysis 51 (2008) 68–75.
[11] Z. Ji, A.F. Jalbout, J.Q. Li, Solid State Communications 142 (2007) 148–153.
[12] Z. Liu, J.E. Hu, Q. Wang, K. Gaskell, A.I. Frenkel, G.S. Jackson, B. Eichhorn, Journal of the American Chemical Society 131 (2009) 6924–6925.
[13] J.G. Wang, B. Hammer, Journal of Catalysis 243 (2006) 192–198.
[14] Y. Ishikawa, M.S. Liao, C.R. Cabrera, Surface Science 513 (2002) 98–110.
[15] T.E. Shubina, M.T.M. Koper, Electrochimica Acta 47 (2002) 3621–3628.
[16] S. Zafeiratos, G. Papakonstantinou, M.M. Jacksic, S.G. Neophytides, Journal of Catalysis 232 (2005) 127–136.
[17] J. Greeley, M. Mavrikakis, Catalysis Today 111 (2006) 52–58.

[18] K.C. Kwiatkowski, S.B. Milne, S. Mukerjee, C.M. Lukehart, Journal of Cluster Science 16 (2005) 251–272.
[19] D.C. Grenoble, M.M. Estadt, D.F. Ollis, Journal of Catalysis 67 (1981) 90–102.
[20] J.A. Rodriguez, R. Liu, J. Hrbek, M. Perez, J. Evans, Journal of Molecular Catalysis A: Chemical 281 (2008) 59–65.
[21] M. Boudart, Chemical Reviews 95 (1995) 661–666.
[22] A.A. Phatak, N. Koryabkina, S. Rai, J.L. Ratts, W. Ruettinger, R.J. Farrauto, G.E. Blau, W.N. Delgass, F.H. Ribeiro, Catalysis Today 123 (2007) 224–234.
[23] H.J. Tian, C.A. Roberts, I.E. Wachs, Journal of Physical Chemistry C 114 (2010) 14110–14120.
[24] M.C. Abello, M.F. Gomez, O. Ferretti, Applied Catalysis A 207 (2001) 421–431.
[25] R. Thomas, E.M. Vanoers, V.H.J. Debeer, J. Medema, J.A. Moulijn, Journal of Catalysis 76 (1982) 241–253.
[26] J.R. Regalbuto, J.W. Ha, Catalysis Letters 29 (1994) 189–207.
[27] R. Thomas, E.M. Vanoers, V.H.J. Debeer, J.A. Moulijn, Journal of Catalysis 84 (1983) 275–287.
[28] J.W. Niemantsverdriet, Spectroscopy in Catalysis: An Introduction, John Wiley & Sons, 2007.
[29] P. Dietrich, R. Lobo-Lapidus, T. Wu, A. Sumer, M. Akatay, B. Fingland, N. Guo, J. Dumesic, C. Marshall, E. Stach, J. Jellinek, W. Delgass, F. Ribeiro, J. Miller, Topics in Catalysis 55 (2012) 53–69.
[30] L. Brewer, R.H. Lamoreaux, in: T.B. Massalski, H. Okamoto (Eds.), Binary Alloy Phase Diagrams, ASM International, 1990, p. 2650.
[31] H.P. Rooksby, B. Lewis, Journal of LessCommon Metals 6 (1964) 451–460.
[32] L.C. Grabow, A.A. Gokhale, S.T. Evans, J.A. Dumesic, M. Mavrikakis, Journal of Physical Chemistry C 112 (2008) 4608–4617.
[33] N. Guo, B.R. Fingland, W.D. Williams, V.F. Kispersky, J. Jelic, W.N. Delgass, F.H. Ribeiro, R.J. Meyer, J.T. Miller, Physical Chemistry Chemical Physics 12 (2010) 5678–5693.
[34] J.H. Pazmiño, M. Shekhar, W. Damion Williams, M. Cem Akatay, J.T. Miller, W. Nicholas Delgass, F.H. Ribeiro, Journal of Catalysis 286 (2012) 279–286.
[35] N.M. Schweitzer, J.A. Schaidle, O.K. Ezekoye, X.Q. Pan, S. Linic, L.T. Thompson, Journal of the American Chemical Society 133 (2011) 2378–2381.